A 2-D Immersed Boundary Method on Low Reynolds Moving Body

Jonas Pereira
jonas.pereira@ist.utl.pt

Instituto Superior Técnico, Lisboa, Portugal

June 2014

Abstract

In this present work the development, the implementation and the results interpretation of an Immersed Boundary Method, in a bi-dimensional Cartesian grid are shown. Three interpolations for the Immersed boundary correction were implemented and tested in a cavity flow with analytical solution. The second order of convergence from the FV discretization was obtained with a polynomial regression using material points and neighbor fluid cells based on the Least Square Method. The verification of the model was performed by comparison of the obtained results with computational data from the literature in steady laminar flows. Both qualitative and quantitative features of the flow were considered and showed considerable resemblance with the literature. In the moving boundary chapter verification was achieved by comparison with both experimental and computational data. The developed code allowed applications for computational modeling of moving boundaries immersed in fluid flows, accurately representing the behaviour of the fluid and the interactions between the fluid and the body's structure. The study of a portion from a winding Eucalyptus peel tube, one of the most common reasons for the propagation of forest wild fires, is performed and the aerodynamic drag force is shown. The comparison of the results with both empiric and computational data confirmed that the method is reliable to solve problems of immersed boundaries and that the computational cost can be decreased for this type of calculations.

Keywords: Immersed Boundary Method, Moving boundary problem, incompressible flows, finite volume method, Least Squares Method

1. Introduction

The subject of this thesis is the application of numerical finite Volume method to moving bodies using the immersed boundary method.

This work comes from the author's interest to increase his knowledge after an academic cycle wherein the fluid dynamic and energy transfer topics have been catching the author's attention.

The fact that in the 21^{st} century the aerospace industry is still relying in static analysis to study temporal variant phenomena leading to extrapolative and inductive reasoning enhanced the author's motivation to build a tool that could be able to provide the desired stability, efficiency and accuracy not only for computational analysis of complex or arbitrary geometries but also to study the behavior of immersed bodies with user prescribed motion and studies where the dynamic and mechanical behavior of an immersed body is ruled by the interaction between the fluid and the body's structure.

It was also important to provide a study of convergence for second order of the immersed boundary method with verification of 2-D results with literature data for fluid flows and to study the effects of the history of the computational cells in the boundary's motion and the consequent integration of aerodynamic forces in this boundary.

1.1. Applied Method

This method is based on the works from [6] and is established by the representation of the solid body as a set of material points (MP) whose motion is computed with the material point method (MPM), whilst the fluid flow is solved in a background polyhedral mesh. The position and the velocity components of the material points are known throughout the computation.

The fixed grid and the respective points and cells have an algorithm of selection which is implemented in order to first classify all the vertex of the grid as either part of the fluid zone or as part of the solid zone.

Secondly the cells were cataloged in three different groups, a cell with all its vertex in the fluid zone was classified as a fluid cell, in case all vertex of a known cell were in solid zone the respective cell was classified as a solid cell. The third group isn't triv-

ial as the first two and is defined as the cells that have both types of vertex, this type of cell have at least one vertex in the solid zone and the rest in the fluid zone, these cells will be from now on called "*IB cells*". Furthermore the faces from the IB cells that are connected to a fluid cell are marked as "*IB faces*".

Lastly this method performs an interpolation using the values of velocity from the neighboring cells and from the MP in order to obtain the velocity that will be used as a boundary condition. The interpolation could be performed either in a cell-centered or in a face-centered basis. In this specific case the chosen method was a finite-volume scheme so the collocation of the values in the faces of the IB cells would be more convenient. So in this method we use a set of velocity values from either material points in the geometrical boundary and neighboring cell's centers in order to interpolate the value of the IB face's velocity components.

2. Background

The features that distinguishes the interpretation of the immersed boundary conditions is the fact that the computational boundary is not geometrically coincident with the physical boundary. So in order to maintain the accuracy of the results an interpolation of the velocity field must be made and this value will then be the fixed value of a Dirichlet BC on the computational boundary.

After the identification of the boundary cells and the discretization of the continuity and momentum equations with a finite volume scheme, the interpolation above mentioned is used to calculate the face center values of the velocity, which do not exist as, in the finite volume schemes the velocity is stored in the cell center. In this work three types of interpolations, with different truncation error orders were used.

In the interpolations algorithms some material points were used and so a routine that can retrieve the closest solid points to the boundary faces, and their coordinates was implemented and executed.

2.1. First Order Interpolation - Interpolation 0

This interpolation scheme is the simplest and is based on the collocation of the closest solid point value in the face value of the immersed boundary. So for every immersed boundary face the above mentioned algorithm selects the closest solid point and uses its value on the boundary face, as in equation 1.

$$\phi_f = \phi_s \tag{1}$$

2.2. Linear Interpolation with Distance Weighting Factor - Interpolation 1

The linear interpolation with the distance weighting is made by the use of two points, one solid and one fluid and is of the form:

$$\phi_f = \phi_c\,(1-\eta) + \eta\phi_s \tag{2}$$

where ϕ_f represents the interpolated value for the face center variable, ϕ_c the cell center value for the variable in question for the cell containing the boundary face, ϕ_s represents the value of the variable in the solid material point closer to the immersed boundary face in question, in the end η represents the weighting factor of the interpolation and can be defined as :

$$\eta = \frac{d_1}{d_1 + d_2} \tag{3}$$

where d_1 represents the distance from the cell center to the face center and d_2 is defined as the distance between the computational boundary face center and the closest material point in solid region.

2.3. Second Order Interpolation with a Quadratic Polynomial obtained with the Least Square Method - Interpolation 2

The two previous subsections described two different approaches to obtain the face value of velocity in the boundary face, but they have at the most a first order of accuracy. The first (subsection 2.1) is really outdated as it was the interpolation scheme used in the earlier computational fluid dynamics calculations and the second one even tough is better still has only a first order of accuracy. In order to obtain a breakthrough a second order interpolation was needed and based on the work of [6] this interpolation was implemented in the SOL software.

In order to obtain a second order of accuracy interpolation scheme a quadratic polynomial of the following form has been created:

$$\phi_f = \beta_0 + \beta_1 x + \beta_2 y + \beta_3 x^2 + \beta_4 y^2 + \beta_5 xy \tag{4}$$

where the β_n coefficients are determined by the least square method. This method was chosen because it gives the user the possibility to obtain an approximated solution for a problem with more equations than unknowns.

The polynomial in equation 4 was formed using a stencil with some of the velocity values of the nearest neighbor cells, with shared vertex with the boundary face, and with the closer of the material points. These points have a prescribed velocity vector, the velocity of the moving boundary, and in case a neighbor cell is an IB cell, the nearest material point to that IB face is taken in account to the construction of the stencil.

As there is variation in the number of IB faces near the interpolated face a selection algorithm was implemented in order to choose the number of solid

or material points in the stencil. The dimension of the stencil varies for each IB face.

After choosing the points of the stencil the construction of the matrices and vectors for the least square interpolation was performed. For the polynomial construction the velocity of every point can be approximated in a matrix form of the equation 4 by $M\vec{\beta}$ where $\vec{\beta} = [\beta_0, \beta_1, \beta_2, \beta_3, \beta_4, \beta_5]^T$ and M:

$$M = \begin{bmatrix} 1 & x_1 & y_1 & x_1^2 & y_1^2 & y_1 x_1 \\ 1 & x_2 & y_2 & x_2^2 & y_2^2 & y_2 x_2 \\ \vdots & \vdots & \vdots & \vdots & \vdots & \vdots \\ 1 & x_n & y_n & x_n^2 & y_n^2 & y_n x_n \end{bmatrix} \quad (5)$$

where n is the number of points of the stencil, that must be at least 6. In the least square method the β_i values are calculated in order to minimize the square of the difference between the real variable ϕ and the interpolated value, so the objective is to get the minimization of $\|\phi - M\vec{\beta}\|^2$. The works of [4] showed that this difference is minimized when the β coefficients are obtained as:

$$\beta = \left(M^T \cdot M\right)^{-1} M^T \phi \quad (6)$$

A correction is necessary in order to maintain the continuity equation and to prevent the interpolation to inject mass in to the system. This correction is a multiplication of the negative fluxes by a ratio $\left(R = \frac{\sum U^+}{\sum U^-}\right)$. This correction is applied before the momentum equations are solved, in order to maintain mass conservation in the domain.

The algorithm of implementation of the second order polynomial using the least square method can be summarized as:

1. Identify the stencil's points, using the method explained above.

2. Obtain the coordinates of the selected cell's centroids as well as the material points coordinates in IB face centered referential.

3. Construct the M matrix obtaining the values of x and y of the velocity

4. Computation of the β coefficients using equation 6 with the M matrix and the velocity values of the previous outer iteration.

5. Apply the mass flux correction in order to maintain the mass conservation.

As the referential used was an IB face centered the value of $\phi_f = \beta_0$ and no further calculations were needed.

3. Results

3.1. Analytical Cavity

The interpolation schemes were tested for the boundarys correction using an analytical solution for a cavity flow in order to assert if it was possible to maintain the global discretization order of the Finite Volume.

The error field for the second order interpolation can be observed in figure 1. It's observable in this figure, in the case of the u component, that the error distribution is similiar to the distribtution of the analytical case solved with FV, what can be interpreted as good indicator that the method is indeed valid. In the v component we can see a zone near the boundary with a high error (red zone), but this can be explained by the fact that even for the analytic cavity case the zone for the highest error is located on the same place as the immersed boundary is in this case, this occurs because the order of magnitude of the v component is almost one scale (10^{-1}) lower, what leads to a higher dispersion of the error field on the domain. We can see the error

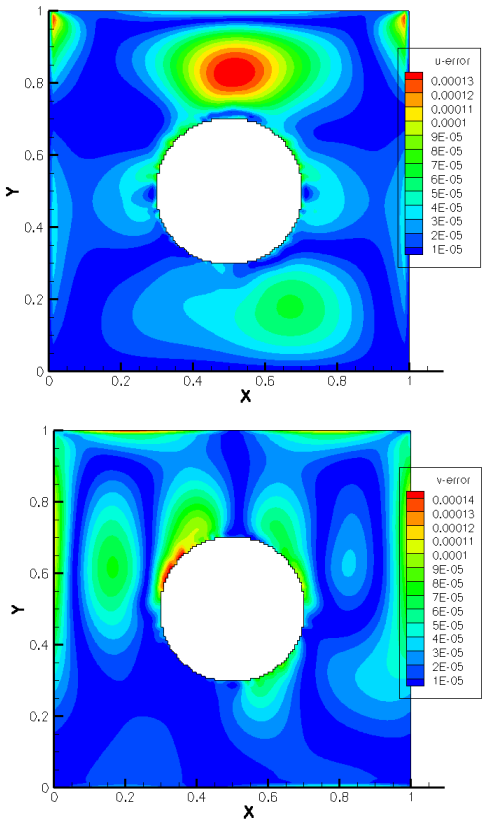

Figure 1: Velocity Error Field for the 160x160 Grid with Interpolation 2

summary in table 3.1. It is worth noticing that in this case the error values are closer to the values obtained by the FV solution for the analytical cavity, where the maximum deviation in the error is found on the mean error in u component, $\bar{\varepsilon}_u$. For

Grid	80x80	160x160
Hydraulic Diameter	1.08E-2	5.44E-3
$\overline{\varepsilon}_u$	9.10E-5	2.70E-5
ε_{umax}	5.05E-4	1.42E-4
$\overline{\varepsilon}_v$	1.02E-4	2.50E-5
ε_{vmax}	5.82E-4	1.52E-4

Table 1: Values the maximum and mean error for both components of velocity in the Analytical Cavity case with immersed boundary and interpolation 2

the other errors we have for ε_{umax}, $\overline{\varepsilon}_v$, ε_{vmax} the deviation between the value with interpolation 2 and without IB is 3% , 22% and 1.9% respectively, for the most refined grid. This meaning that for the maximum errors the two computations have almost identical errors.

Using figure 2 we can assert the premise that this interpolation is second order accuracy, as the exponential value of the decrease of the error with the hydraulic diameter of the grid is almost 2, as can be seen in table 3.1.

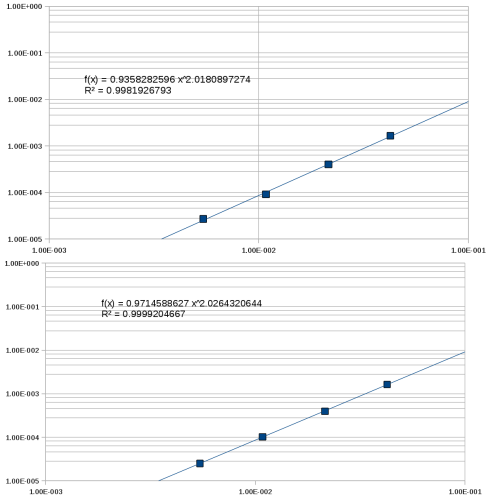

Figure 2: Decay of the mean error with the hydraulic diameter of the grid with Interpolation 2, on the left for th u component of velocity and on the right for the v component

Error	p2
$\overline{\varepsilon}_u$	2.018
ε_{umax}	1.955
$\overline{\varepsilon}_v$	2.026
ε_{vmax}	1.937

3.2. Reynolds 40

The steady laminar flow of $Re = 40$ around the circular cylinder is the main section of the steady immersed boundaries results. The bibliographic data for this particular case was more extensive than for the previous case, thus making the comparison of results and its consequent validation easier. This flow was expected to be a steady laminar flow. In figures 3 we can observe the distribution of the pressure coefficient along the perimeter of the body and in figure 4 the fricition coefficient.

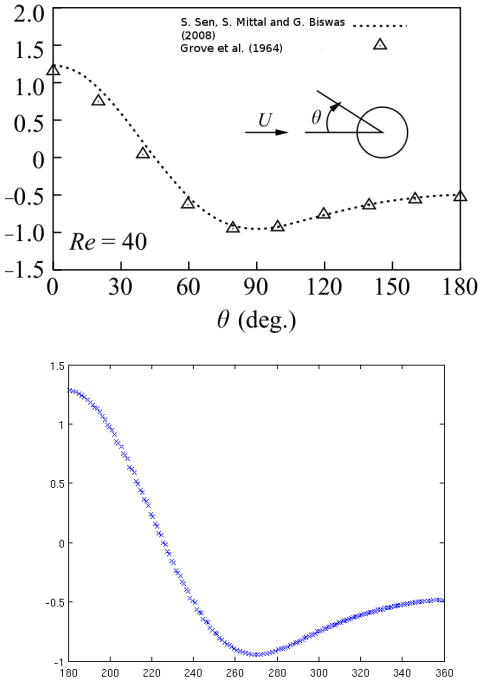

Figure 3: Image taken from [7]-pp 97, representing the distribution of the pressure coefficient along θ on the left. On the right Distribution of pressure coefficient ,c_p with θ obtained with most refined grid, fine-tail

With an immediate observation of figure 3 we can understand the similarities between the results. The main difference can be pointed out as a small difference in the c_p value over the leading edge is a little higher than the values shown in the bibliography.
This small discrepancy over the results can be explained with two reasons. The first is the difference in the blockage effect of the computational calculations. In the case of [7] the figure shown represents a domain with a blockage effect of $B = 0.05$ and in our calculations the chosen domain had $B = 0.01$.

The other source for the error comes from the calculations of the pressure around the physical boundary. As the computational boundary is wider than the physical boundary and we only have pressure values for the cell centers an extrapolation was needed in order to obtain the pressure around the cylinder.

This interpolation was effectuated using the values of the pressure gradient in the boundary's faces and the distance of each face center to the closest material point in the physical boundary of the cylinder.

The separation angle θ_{sep} is defined as the angle at which the the boundary layer separates from the boundary, which is represented as the angle at which the friction drag is null. In figure 4 we can notice the friction distribution along θ for the more refined grid on the right and the distribution of the friction coefficient in [2]. It's important to state that as in figure 3 they started to account the angle at the leading edge, and in the computations executed in this work the angle that has a zero value is the trailing edge of the cylinder. Also worth of note, the image of the right has the representation for the whole cylinder and the case from [1] only 180 are shown.

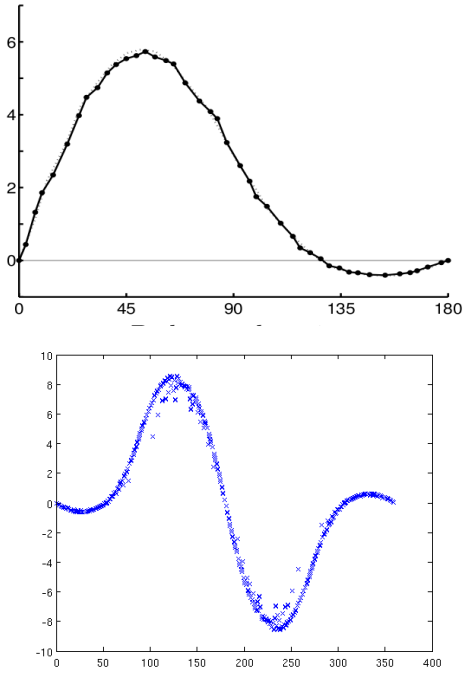

Figure 4: Distribution of friction coefficient ,c_f with θ, on the left for the medium refined grid, on the right picture from [2]-Figure 5.3 D pp 84

In the obtained results the maximum skin friction is higher than the results from [1], the divergence in the results is explained by the fact that the computational boundary is not coincident with the physical boundary, besides that our boundary condition is not a true wall with no slip condition but is almost as a source/sink term in order to correct the distance from the physical boundary to the computational.

But in contrast to the result of the separation angle has an undeniable proximity to our obtained values. This can be viewed in table 3.2. The maximum value of divergence in the more refined grid to the data from the bibliography is nearly 1.2% which is negligible.

source/Grid	L_{sep}	$\theta_{sep}()$	C_d
[2]	2.19	54.2	-
[1]	2.20	53.5	1.713
[2] Empiric Prediction	2.25	53.52	1.51
[7] -Empiric Prediction	-	-	1.51
[8]	2.21	53.5	1.66
coarse tail	2.503	46.85	1.46
medtail	2.525	49.84	1.52
fine tail	2.520	53.55	1.54
notail	2.489	53.55	1.55

Table 2: Results from different bibliographic sources and all grids for $Re = 40$

Regarding the separation angle it's important to state the grid convergence of results for the different grids, being the results for the more refined grids more similar to the bibliographic sources' results. Another item that has to be compared in order to obtain validation to this model is the drag coefficient C_d. As shown in table 3.2 the values for this coefficient are very similar too.

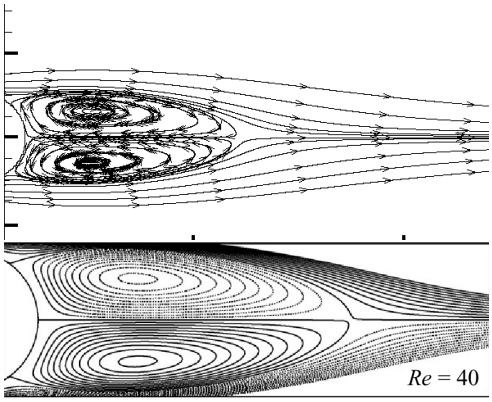

Figure 5: Representation of streamlines in the vicinity of the immersed boundary at $Re = 40$. On the left the results computed with the IBM, on the right figure taken from [7]-figure 6c p 101

In figure 5 we can observe a few streamlines in the wake zone of the cylinder. It is possible to observe too the end of the wake.

Although the figure from the bibliography does not have a scale it is possible to conclude that the behaviour of the streamlines is similar and that even tough the value of L_{sep} has some small differences the overall behaviour of the flow does not act different. The difference in the L_{sep} are justified by the fact that the domains are different between both cases and the outer boundaries are not symmetry

planes but pressure outlet, that implies a higher blockage effect.

3.3. 2-D Horizontally Oscillating Cylinder in a Static Flow

This section presents the results for a simulation of an oscillating moving boundary immersed in a static fluid, with $Re = 100$ for the maximum velocity of the body and a Keulegen-Carpenter number $KC = 5$.

The present results were compared with the data available in [3]. The computational experience performed in this section was carried out in order to reproduce one of the analysis performed in the mentioned literature.

The diameter of the 2-D static cylinder was defined as $D = .02$m, and for a square domain of $[10D]^2$. The center of the body was animated with a sinusoidal motion as described in equation 3.3. The amplitude of the motion was established in order to obtain $Re = 100$ for a $\nu = 10^{-6}$, the frequency of the oscillation was implemented to be equal to the literature. The maximum velocity of the body was a result of the Reynolds number and the Keulegen-Carpenter number and was settled as $U_{max} = 0.005$.

$$x_{center} = 0.159 \ \sin(2\pi 0.05t) \tag{7}$$

In this type of method the Courant must be set with a value that doesn't allow the boundary to move more than one computational cell between time-steps, so the time step chosen for these computations was $dt = 0.1$ and the courant= 1/20.

The pressure and the vorticity isolines for four different phases of a cycle were captured and compared with the computational results of [3], which can be seen in figures 6

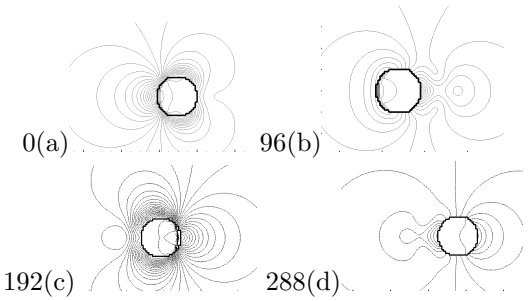

Figure 6: Pressure isolines obtained with the proposed method for four different phases of the periodic motion

In figure 6 we can observe the pressure contours in the computational analysis for four phases of the motion described in the literature.

In order to obtain validation for this method a comparison with empiric results was also necessary. In figure 7 we can observe the comparison of the x component of the velocity for three different phases of the cycle. In each phase of the cycle the velocity was analyzed at two different lines. The velocities were analyzed at $x = -0.6D$ and $x = 1.2D$. There's similar tendency of the experimental data with the results computed with the immersed boundary.

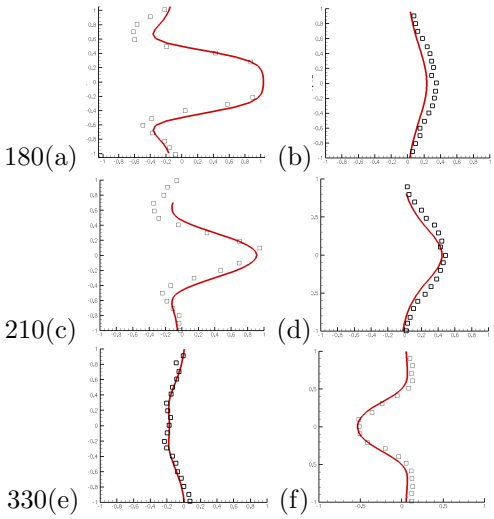

Figure 7: On the left the results for $x = -0.6D$ and on the right $x = 1.2D$. The red line represents the computational results obtain with the IBM and the black squares represent the empirical data from [3], pp 258 figure 6.

The data presented in figure 7a) shows that there's a velocity profile caused by the forward motion of the IB that generates a low pressure zone in its wake thus inducing the velocity in the fluid. This velocity profile is the most intense in all represented frames because of the proximity of the body to the probe in this instant. Another interesting feature of this frame is the negative velocity present at $||y|| > r$, where the negative velocity is induced by the continuity equation, in order to respect the mass balance in the wake of the cylinder .

The second frame has a velocity profile with small intensity, that is caused by the fact that in the moment when those velocities were captured the body was going towards the probe and was still far from it.

At the second moment of capture, 210 we can observe that the intense velocity profile from frame 7a) is dissipating as the body moves away from the probe while at the $x = 1.2D$ location the velocity profile is starting to get preponderance as the body moves closer to the probe.

Finally when the IB reaches 330 the body is in the same place as it was in previous frames but in this case it's moving backwards. The velocity profile shown in figure 7 f) is caused by the low pressure zone inherent to the wake of the body. The lower intensity of this frame compared to the first

Force	Average	Maximum	Minimum
Drag (N)	21.31	25.02	15.97
Lift (N)	-0.59	4.235	-5.94

Table 3: Values for the avarege, minimum and maximum values of the aerodynamic forces for the flattened cylinder case

is caused by the distance of body to the probe in the moment of the capture of the velocities.

At last in figure 7e) we have a similar behavior to frame b), as the body is moving towards the probe but it's still far away.

3.4. Rotating Flattened Cylinder

One of the advantages of this type of algorithms in the resolution of flows around immersed boundaries is the possibility to perform analysis with arbitrarily defined bodies without the requirement of creating a new computational mesh, unlike the case of body-fitted grids.

This shape was defined by 3 semi-circles, one with radius equal to $r = 0.01$ and the other two with half of the radius. This geometry was chosen in order to have a simplified model of a section from winding Eucalyptus peel tube, one of the most common reasons of the propagation for forest wild fires.

This part of work was mainly motivated as part of an ongoing investigation regarding forest fires. The premisses of this investigation was that the winding Eucalyptus peel was usually animated with an angular frequency of $10Hz$ which meant an angular velocity of $\omega = 20\pi\ /s$. We computed our solutions for a $Re = 40$.

Once again we expected a periodic solution for this flow. Although we were on a steady laminar domain, as can be seen in section 3.2 the asymmetry of the body and the rotation imposed on it made us expect that the perturbations induced on the fluid would have a sinusoidal behavior. In figures 8 we can see the pressure distribution for four phases of a period, namely $\theta = 0$, $\theta = \frac{\pi}{4}$, $\theta = \frac{1\pi}{2}$, $\theta = \frac{3\pi}{4}$.

In these 4 frames it's possible to observe that the pressure around the immersed boundary is changing with the position of the flattened half of the body. From those frames we can remark that in 8a) the peak of pressure in the stagnation point is lower that in the other phases of the motion. Just as the pressure in the leading edge varies with time the distribution of the pressure in the rest of the boundary is also changing accordingly which will produce a temporal variation in the aerodynamic forces. In table 3 we have the minimum, maximum and average values for the aerodynamic forces of this case.

Another interesting fact present in figure 8 is the

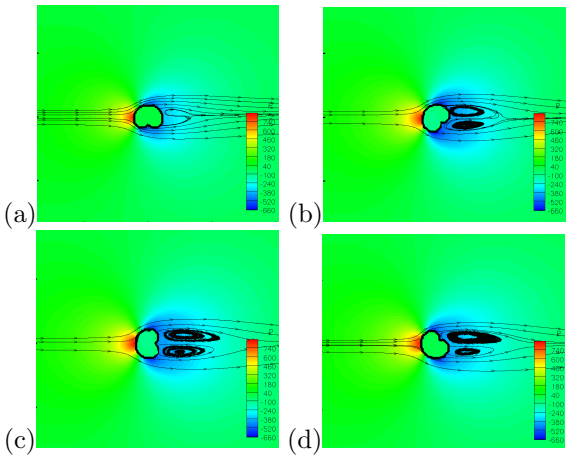

Figure 8: 4 phases of the distribution of pressure for one cycle of the flattened cylinder at $Re = 40$ and $f = 10Hz$, and streamlines representation

variation of the streamlines with the rotation of the body. We can see in 8a) that the vortex is really small and in the following 8b) and 8c) there a development of the vortexes until figure 8d) is reached, where the vorticity starts decreasing.

When we reach the second half of the motion we once again there's formation of vorticity but in this case the length of recirculation is larger. The vortexes that were formed in the first half of the cycle are dissipated by the rotation of the body.

The evolution of streamwise aerodynamic force is not a pure harmonic there's the presence of a local maximum in each period. This local maximum is explained by the asymmetry of the body. When the flattened half of the body is in the trailing edge the surface exposed the wake behaves like a cylinder of radius equal to the radius of the bigger semi-circle. In the other halve of the period the behaviour is influence by the complexity of the geometry.

3.5. Free Motion of 2-D Cylinder Inside a Cavity

Another example of a possible application for this method, and similarly for the computational tool implemented in the SOL-code is to obtain the results of the behaviour of an immersed body inside a chamber with a circular flow. The most representative flow of this type is the flow inside a whistle, having the behaviour of the fluid flow the interaction between it and the small sphere inside the chamber.

In our literature survey we were able to understand that noise produced by a whistle is a result of the exit jet break down, shedding creates the acoustic characteristic field of the whistle. The interaction between the immersed cylinder inside the chamber as explained in [5] is not the dominant effect but it modulates and destabilizes the output jet that typically impinges in a blade to create the

shedding mechanism.

The tool was only developed for 2-D idealized case, so instead of a sphere inside a 3-D chamber we simplified the problem for a bi-dimensional flow inside a chamber with a 2-D circular cylinder inside.

This domain has one particularity, the mass flow that comes from the inlet is going directly to the outlet and the flow inside the chamber is created with the shear stress from the stream going to the outlet. This shear layer is accelerating the steady flow inside the chamber will have an influence in the pressure around the immersed body, this pressure differential will then force the body to move.

The behaviour of the body is computed with the dynamic laws of motion after the integration of the pressure and shear stress in the whole boundary, that is obtained by the resolution of the Navier-Stokes equations for the fluid region of the domain.

The collisions between the IB and the chamber's walls were computed as elastic collision with $e = 1$. A simplification had to be performed because when the boundary was close to the limits of the domain, when there was less than two cells between boundaries, a pressure peak would be present in these cells making the method fail to converge.

In order to solve this problem an offset for the fixed boundaries was programmed to the code. Resuming every time the distance between the immersed body and the one of the fixed walls was lower than $\epsilon = 0.003$, which corresponds to three cells, an elastic collision was simulated and the the body's velocity component that was perpendicular to the fixed wall switched sign.

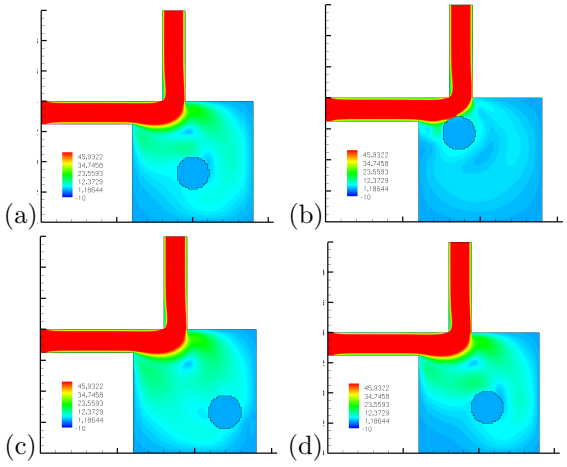

Figure 9: Four frames represent two periods of the quasi-cyclic behavior of the IB inside the whistle, velocity magnitude

With figure 9 we are able to understand the behavior of the immersed boundary inside the chamber as these four frames represent two cycles of the body's dynamic.

In the first frame 9a) the IB is at center of the chamber and starts moving towards the high momentum and low pressure zones, represented in red. When the IB reaches this high momentum zone , it creates a low pressure zone in the trailing edge, observable in the dark blue bubble, thus projecting the immersed boundary.

The momentum gained in the projection is high enough for the IB to reach the chamber's wall and therefore collide with it, the moment before this collision is represented in c) as the IB is moving towards the wall, and in d) the IB is moving away from the wall.

After the collision and the dissipation of the momentum gained in frame b) the cylinder repeats the behavior as it is sucked to the low pressure zones and cycle continues.

4. Conclusions

The IBM was implemented in an unstructured finite volume code and several verification and validation tests were undertaken.

Three different interpolation schemes for the boundary's correction using an analytical solution in order to assert if it was possible to maintain the global discretization order of the Finite Volume.

From this analysis we were able to conclude that if the polynomial used in the correction of the immersed boundary is of the same order (in this case second order) of the discretization method it is possible to obtain the FV global second order of accuracy. This polynomial was constructed using solid material points and the cell centroids from the fluid cells where the correction was supposed to be implemented. The polynomial is obtained using a regression based on the Least Square Method.

Analysis for flows with $Re = 40$ with an immersed 2-D cylinder were performed with an effective success in both fields, the qualitative and quantitative. For these cases we were able to obtain results for the separation angle, θ_{sep}, drag's coefficient, C_D, and for length of the wake zone, L_{circ}. These results have shown a good relation with the results from the literature. The pressure distribution and the shear stress alongside the cylinder were computed and a comparison with the ones from the literature was also successful. In order to obtain the pressure distribution and the shear stress along the immersed boundary we had to implement a tool for the extrapolation of these quantities from the neighbor fluid cells to the solid material points.

The IBM was applied to a moving boundary for a periodic case experimentally investigated by [3]. The pressure and vorticity contours as well as the the velocity at different positions in different time instants were compared with the computational and the empirical data available. The comparison of this

values was satisfactory thus asserting the validation of the method.

Finally the IBM was applied for the case of a rotating Eucalyptus peel tube with an incoming flow at $Re = 40$ in order to study the aerodynamic behaviour of this complex geometry and to a 2-D cylinder moving frelly in a cavity flow that was the simplification of a whistle with an immersed body inside its cavity. The dynamic laws of motion were used based in the aerodynamic forces resultants from the interaction between the fluid and cylinder. These dynamic laws included the ellastic collisions of the cylinder with the wall of the cavity of the computational domain.

The proposed method is reliable to solve problems that include the immersion of a body in a fluid flow and it improves the efficiency using parallel computation producing accurate results at a low computational cost, specially for low Re number flows.

In summary this type of method is in an area of computational mechanics that has room for improvement and a promising investment thus providing the aerospace market with powerful tools to analyze the behaviour of bodies immersed in fluids.

4.1. Future Work

An improvement to this method would be evolution to a 3-D domain, since the principles are the same and are already well defined. The current method can also be applied on unstructured grids in application where this feature could be important.

Other future implementations of this method to obtain the behaviour of a body immersed in a turbulent flow with a high Re number,by using either RANS (Reynolds Average Navier-Stokes) or LES (Large Eddy Simulation). This methods are currently being implemented and validated in the SOL-code.

The last suggestions are related with the order of convergence of the method, where adaptivity and high order discretization schemes will improve the results. In the case of high order discretization schemes, it was proven in this work that the only requirement for the immersed boundary correction is that the degree of the least square polynomial needs to be equal or higher than the order of the FV discretization.

References

[1] M. T. Drge. Cartesian grid methods for turbulent flow simulation in complex geometries, 2007.

[2] K. Y. H. Ding, C. Shu and D. Xu. Simulation of incompressible viscous flows past a circular cylinder by hybrid fd scheme and meshless least square-based finite difference method. *Computational Methods Applied Mechanical Engineering.*, 193:727–744, 2004.

[3] S. B. H. Dutsch, F. Durst and H. Lienhart. Low-reynolds-number flow around an oscillating circular cyllinder at low keulegan-carpenter numbers. *Journal of Fluid Mechanics*, 360,:249–271, 1997.

[4] T. Kariya and H. Kurata. *"Generalized least squares, Wiley Series in Probability and Statistics"*. John Wiley Sons Ltd., 2004.

[5] J. Liu. Simulation of whistle noise using computational fluid dynamics and acoustic finite element simulation, 2012.

[6] L. S. Sanjay R. Mathur and J. Y. Murthy. An unstructured finite-volume method for incompressible flows with complex immersed boundaries. *Numerical Heat Transfer, Part B: Fundamentals: An International Journal of Computation and Methodology*, 58(4):217–241, Oct. 2010.

[7] S. M. Subhankar Sen and G. Biswas. Steady separated flow past a circular cylinder at low reynolds numbers. *Journal of Fluid Mechanics*, 620:89–119, 2009.

[8] S. Xu and Z. J. Wang. An immersed interface method for simulating the interaction of a fluid with moving boundaries. *Journal of Computational Physics*, 216,:454–493, 2006.